Author(s): Bronis, A.; Heßberger, F. P.; Antalic, S.; Andel, B.; Ackermann, D.; Heinz, S.; Hofmann, S.; Khuyagbaatar, J.; Kindler, B.; Kojouharov, I.; Kuusiniemi, P.; Leino, M.; Lommel, B.; Mann, R.; Nishio, K.; Popeko, A. G.; Streicher, B.; Sulignano, B.; Uusitalo, J.; Venhart, M.; Yeremin, A. V.

Title: Decay studies of new isomeric states in 255No

Year: 2022

Version: Published version

Please cite the original version:

Bronis, A., Heßberger, F. P., Antalic, S., Andel, B., Ackermann, D., Heinz, S., Hofmann, S., Khuyagbaatar, J., Kindler, B., Kojouharov, I., Kuusiniemi, P., Leino, M., Lommel, B., Mann, R., Nishio, K., Popeko, A. G., Streicher, B., Sulignano, B., Uusitalo, J., . . . Yeremin, A. V. (2022). Decay studies of new isomeric states in 255No. Physical Review C, 106(1), Article 014602. https://doi.org/10.1103/PhysRevC.106.014602

Decay studies of new isomeric states in ^{255}No

A. Bronis,[1,*] F. P. Heßberger,[2,3] S. Antalic,[1] B. Andel,[1] D. Ackermann,[4] S. Heinz,[2] S. Hofmann,[2] J. Khuyagbaatar,[2,3] B. Kindler,[2] I. Kojouharov,[2] P. Kuusiniemi,[5] M. Leino,[5] B. Lommel,[2] R. Mann,[2] K. Nishio,[6] A. G. Popeko,[7] B. Streicher,[2] B. Sulignano,[8] J. Uusitalo,[5] M. Venhart,[9] and A. V. Yeremin[7]

[1]*Department of Nuclear Physics and Biophysics, Comenius University in Bratislava, 84248 Bratislava, Slovakia*
[2]*GSI Helmholtzzentrum für Schwerionenforschung, GmbH, 64291 Darmstadt, Germany*
[3]*Helmholtz Institut Mainz, Johann-Joachim-Becherweg, 55128 Mainz, Germany*
[4]*GANIL, CEA/DSM-CNRS/IN2P3, Bd Henri Becquerel, BP 55027, F-14076 Caen Cedex 5, France*
[5]*Department of Physics, University of Jyväskylä, P.O. Box 35, FI-40014 Jyväskylä, Finland*
[6]*Advanced Science Research Center, Japan Atomic Energy Agency, Tokai-mura, Ibaraki 319-1195, Japan*
[7]*Joint Institute for Nuclear Research, 141980 Dubna, Russia*
[8]*Irfu, CEA, Université Paris-Saclay, F-91191 Gif-sur-Yvette, France*
[9]*Institute of Physics, Slovak Academy of Sciences, 84511 Bratislava, Slovakia*

(Received 17 February 2022; revised 11 May 2022; accepted 25 May 2022; published 5 July 2022)

The decay of excited states in ^{255}No was investigated by applying the evaporation-residue–conversion-electron correlation technique. Two new isomeric states were observed in ^{255}No together with the previously known one. Excitation energies of the isomeric states were estimated based on the energies of conversion electrons and γ rays from correlation chains. These results were in accord with theoretical calculations based on the mean-field models. A tentative decay scheme of isomeric states in ^{255}No is proposed, and their Nilsson configurations are discussed. The energy decrease of the $11/2^-$[725] Nilsson level for heavy $N = 153$ isotones as a function of increasing proton number is confirmed.

DOI: 10.1103/PhysRevC.106.014602

I. INTRODUCTION

Single-particle level energies are often estimated by theoretical models with various parametrizations when experimental data are missing. In general, typical approaches include self-consistent [1,2] or macroscopic-microscopic (mac-mic) models [3,4]. Mainly the latter seem to adequately describe the order and energies of single-particle levels in general, specifically in the region of heavy even-Z, $N = 151$ and $N = 153$ isotones. However, in the case of the $11/2^-$[725] Nilsson level, experimental observations deviate significantly from predictions of mac-mic models. Experimental energies of this level appear to be relatively stable from ^{249}Cm to ^{253}Fm forming low-energy short-lived isomeric states in these isotopes, decaying via internal transition. This plateau of the $11/2^-$[725] state is followed by a steep decrease of its excitation energies for $N = 153$ isotones at $Z > 102$, having a significant impact on their half-life and decay mode. In the isotope ^{257}Rf, the half-life of the $11/2^-$[725] level is comparable to the half-life of the ground state (g.s.). As a result, it undergoes α decay. The decrease of $11/2^-$[725] excitation energy continues in ^{259}Sg, where it becomes the configuration of the ground state [5]. In contrast to such rapid reduction in excitation energy, only a smooth decrease of its energy from ^{249}Cm up to ^{261}Hs is predicted. According to experimental systematics, the turning point of the $11/2^-$[725] Nilsson level from ^{253}Fm to ^{257}Rf in $N = 153$ isotones is ^{255}No. Localization of its $11/2^-$[725] state is an important addition to complete the systematics, especially as the plateau of $11/2^-$[725] level excitation energy corresponds to the predicted maximum of quadrupole deformation [6].

The isotope ^{255}No was identified for the first time in 1967 by Ghiorso *et al.* [7]. Since then, studies have been mainly focused on its α decay, which populates a low-energy isomeric state in the daughter nucleus ^{251}Fm [8–10]. After 50 years since the identification of ^{255}No, only the low-energy $3/2^+$[622] Nilsson level populated via α decay of ^{259}Rf [11] and a tentatively assigned isomeric state are known. The latter was suggested on the basis of the 741- and 839-keV γ transition half-lives of 105 ± 25 and 130 ± 25 μs [12]. The investigation of the ^{255}No deexcitation scheme and its isomeric states usually encounters difficulties related to the utilized reaction. Employment of the highly asymmetric reaction ^{238}U(^{22}Ne, xn)$^{260-xn}$No suffers from low velocities of recoiling nuclei, resulting in a broad angular distribution and thus low transmission values using recoil separators. In the more symmetric reaction ^{208}Pb(^{48}Ca, xn)$^{256-xn}$No the main complication is the "contamination" by ^{254}No, being produced with similar or higher cross section. Long half-lives of both isotopes and partially also the overlap of the most intense α-decay energies in ^{254}No ($E_\alpha = 8096 \pm 10$ keV [12]) and ^{255}No ($E_\alpha = 8095 \pm 10$ keV [8]) make their discrimination challenging. Additional complications arise

*adam.bronis@fmph.uniba.sk

from the presence of two known isomeric states in ^{254}No. In such a case, we could make the distinction of ^{255}No and ^{254}No on the basis of two experiments with different production cross-sections of each isotope at two different beam energies. Comparison of partial cross-section ratios of ground and isomeric states from both experiments allowed us to discriminate between ^{254}No and ^{255}No isomeric states. A similar approach was used, for example, in the investigation of ^{255}Lr and ^{256}Lr [13].

II. EXPERIMENT

Two experiments using the same projectile-target combination were performed at GSI in Darmstadt, Germany. The first experiment aimed at the investigation of ^{255}No α decay (Exp1) used a kinetic energy of $E_{\rm lab} = 213.6$ MeV for ^{48}Ca projectiles. The second experiment (Exp2) was focused on a detailed study of isomeric states in ^{254}No using a higher projectile energy ($E_{\rm lab} = 218.4$ MeV). Additional information on Exp1 and Exp2 is given in Table I.

In both experiments, the ^{48}Ca beam was delivered by the ECR ion source followed by the UNILAC accelerator. The isotopically enriched target material ^{208}PbS with a thickness of 450 μg/cm^2 was evaporated on a 40 μg/cm^2 carbon layer facing the beam. Another 10 μg/cm^2 carbon layer was positioned downstream for better radiation cooling. The targets were installed on a wheel, which rotated synchronously to the beam macrostructure (5 ms pulse with 50 Hz repetition frequency). Reaction products were separated from the primary beam by the velocity filter SHIP [14] and focused onto the detector system positioned at the focal plane of the separator. The evaporation residues (ER) were implanted into a position-sensitive 16-strip passivated ion-implanted silicon detector (STOP det.) [15]. In front of the STOP detector, a six-segment (two vertical and four horizontal), 32-strip silicon detector with box geometry (BOX det.) was placed to measure particles escaping from the STOP detector into the backward hemisphere [15]. Energy calibration of both silicon detectors was performed using α-decay energies of ^{254}No and the decay products ^{250}Fm and ^{246}Cf. The energy resolution of the STOP detector was 30–32 and 23–25 keV (FWHM) in Exp1 and Exp2, respectively.

Behind the STOP detector, a high-purity germanium (HPGe) clover detector was arranged to measure γ and x-rays emitted within time differences of Δt(particle-γ) <5 μs or Δt(particle-γ) >25 μs with signals from the STOP or BOX detectors. We refer these types of events as coincidences [Δt(particle-γ) <5 μs] or correlations [Δt(particle-γ) >25 μs]. Different types of HPGe clover detectors (mounted in close geometry, covering the complete area of the STOP detector), were used in the two experiments (Table I). For Exp1, a VEGA type detector was used, consisting of four crystals with a diameter of 70 mm and a length of 140 mm, assembled in a block (124 × 124 × 140) mm^3 [16]. The same geometry was used in Exp2 for the SHIP Clover, wherein each crystal had a diameter of 50–55 mm and a length of 70 mm with volume (102 × 102 × 70) mm^3. Time differences [Δt(particle-γ)] below 5 μs were measured by a TAC (STOP-Ge) (time to amplitude converter). A continuously running clock was used in the region above 25 μs. Time resolutions were ≈200 ns in the first and ≈1 μs in the second interval, respectively. Energy calibration of the clover detectors was performed by use of external γ-ray sources of ^{152}Eu and ^{133}Ba with an accuracy of ±0.5 keV. The relative efficiency was obtained using the same sources in both experiments. Further details of calibration and absolute efficiencies in Exp1 and Exp2 are given in Refs. [17] and [12], respectively.

TABLE I. Conditions of experiments in the decay study of the ^{255}No isomers. Beam energy ($E_{\rm lab}$), excitation energy (E^*), beam intensity (I), duration of the irradiation (Time) and cross section (σ) for the production of ^{255}No are given for each experiment. Excitation energies (E^*) correspond to the production in the middle of the target, "Ge det." stands for the type of clover detector used as described in Sec. II.

Exp.	$E_{\rm lab}$ (MeV)	E^* (MeV)	I (pμA)	Time (h)	Ge det.	σ (nb)
Exp1	213.6	17.3	1.1	18	VEGA	≈400
Exp2	218.4	21.3	0.8–1.3	19	SHIP	≈120

III. RESULTS

In both experiments the production of ^{255}No was significantly lower in comparison to ^{254}No and most of its α energies in the range of 7700–8350 keV were overlapping with ^{254}No and could not be resolved (Fig. 1). We attribute the dominant peaks with energies 8088 ± 10 keV and 7429 ± 10 keV to α decays of ^{254}No and ^{250}Fm, respectively. In addition, a few

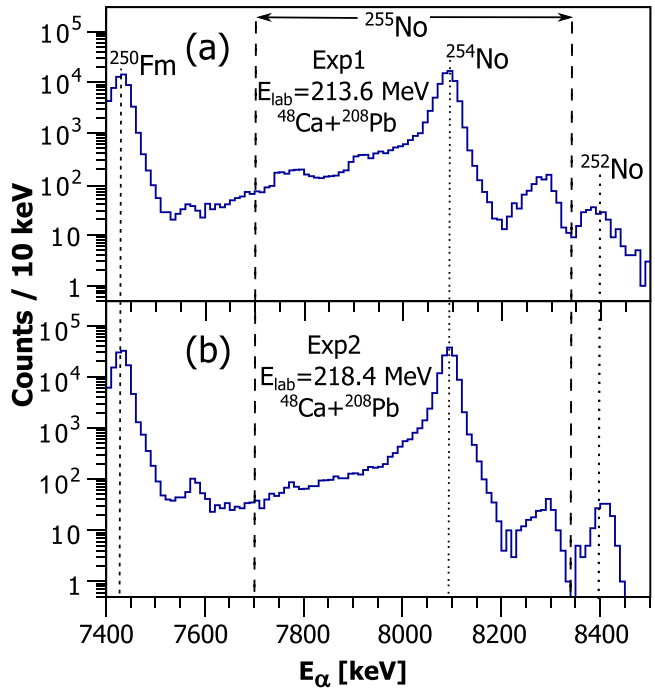

FIG. 1. Energy spectrum of α decays during beam pause in the experiment with projectile kinetic energy of (a) 213.6 MeV (Exp1) and (b) 218.4 MeV (Exp2).

TABLE II. Conditions for different types of correlation search in Exp1 and Exp2. Energy (E_{CE1} | E_{CE2}) and time windows [Δt(ER-CE1) | Δt(CE1-CE2)], number of observed (N_{Exp}) and expected random (N_{Rnd}) correlation chains are given.

Exp.	Corr. chain	E_{CE1} (keV) | E_{CE2} (keV)	Δt(ER-CE1) (ms) | Δt(CE1-CE2) (ms)	N_{Exp}	N_{Rnd}
Exp1	ER-CE	0–900 | ——	0–0.5 | ——	7387	88
	ER-CE1-CE2	0–900 | 0–900	0–1.0 | 0–1.0	465	0.08
Exp2	ER-CE	0–900 | ——	0–0.5 | ——	5387	95
	ER-CE1-CE2	0–900 | 0–900	0–1.0 | 0–1.0	155	0.07

hundreds of ^{252}No nuclei were produced by the reaction of ^{48}Ca with ^{206}Pb impurities in the target material (Fig. 1).

To discriminate decays of isomeric states from a large background of γ rays, we investigated conversion electrons (CEs) produced in deexcitation of an isomeric state via internal conversion, which followed the implantation of ERs [18]. It has to be noted that the CE signal is usually created as a summation of CEs, Auger electrons, and low-energy x rays. This summation is especially important for transitions converted on the L atomic shell because these transitions have significantly higher probability of emission of an Auger electron in comparison to the transitions converted on the K atomic shell [19,20]. In addition, low-energy x rays have higher chance to deposit part of their energy in the silicon detector. Therefore, for estimating the energies of excited states, we assume that endpoints of the CE energy distributions correspond to the full absorption of the energy of converted transitions. We used the time and position correlation method [21] in order to search for ER-CE or ER-CE1-CE2 sequences in both experiments. Because of the low CE energies, their position signals in the individual strip of the STOP detector were often below the detection threshold and thus not registered. Therefore, instead of using position signals, we only required the ER and CE to be registered in the same strip of the STOP detector. The details of the correlation search are summarized in Table II together with the extracted experimental numbers of correlation chains and the estimated numbers of random correlation chains. The latter values were calculated based on ER and CE counting rates according to the method discussed in Ref. [22]. The number of ER-CE or ER-CE1-CE2 events was found to be up to three orders of magnitude higher than the random correlations (Table II). Hence, we ruled out a possible random origin of the ER-CE or the ER-CE1-CE2 sequences.

We evaluated partial cross sections and their ratios based on the number of ER-CE1-CE2 correlation events (Table III). Minor differences in the ratios for different states in the same isotope might reflect the average spin population in the reaction; i.e., the probability of populating high-spin states increases with the energy of the reaction [23]. This phenomenon was also observed in the neighboring nuclei ^{254}No [12] and ^{250}No [24]. The ratios of the ER-CE1-CE2 correlation chains clearly follow the trend of ^{255}No in contrast to ^{254}No (Table III). As a supporting argument for this tendency, we performed HIVAP calculations [25], predicting an increase of ^{254}No cross section by a factor of 7 with the increase of excitation energy from 17.3 to 21.3 MeV. On the other hand, the isotope ^{255}No follows an opposite trend, where a decrease of its cross section by a factor of 6 is obtained. Thus these HIVAP calculations roughly agree with the experimental data given in Table III and we assign ER-CE1-CE2 correlations from both experiments to the deexcitation of isomeric states in ^{255}No.

The γ transitions in coincidence with CEs or ERs from ER-CE chains are presented in Figs. 2(a)–2(c) for Exp1 and Exp2, respectively. We note that considerably higher statistics of ^{254}No was collected in Exp2 as compared to Exp1 [Figs. 2(b) and 2(a)]. Therefore, any γ line observed in Exp1, but not (or with significantly lower intensity) in Exp2, could be attributed to the decay of ^{255}No. Intense K and L x rays of nobelium ($K_{\alpha 1} = 127.36$ keV, $K_{\alpha 2} = 120.95$ keV [26], $L_{\beta 1} = 23.22$ keV [27]) and a 606-keV γ ray attributed to the deexcitation of the ^{254}No^{m2} isomeric state [12] were measured in coincidence with CEs in both experiments [Figs. 2(a) and 2(b)]. In addition, the 632-, 657-, 741-, and 839-keV γ rays were in coincidence with CEs in Exp1 [Fig. 2(a)]. The high-energy 741- and 839-keV γ rays were also observed in Exp2, albeit with significantly lower intensities than in Exp1 [see inset in Fig. 2(b)], and were previously tentatively assigned to deexcitation of an isomeric state in ^{255}No [12]. We found weak K and L x rays of nobelium and 355-, 632-, 700-, 741-, and 839-keV lines in coincidence with ERs in Exp1 [Fig. 2(c)]. In Exp2, only a very weak 741-keV γ transition was observed.

As the next step in our analysis, we searched for ER-CE1-CE2 sequences. To enhance weak transitions, the data from Exp1 and Exp2 were added together. The γ rays with energies 632, 657, 741, and 839 keV, observed already in ER-CE correlations, were coincident with the CE1. Additional lines

TABLE III. Partial cross sections (σ_{Exp}) of ER-CE1-CE2 correlations, ^{255}No, ^{254}No^{m2}, ^{254}No^{m1}, ^{254}No in Exp1 and Exp2 and their ratios ($\sigma_{Exp1}/\sigma_{Exp2}$). The ER-CE1-CE2 correlation chains are assigned to decay of isomeric states in ^{255}No (see text for details).

Isotope	E^* (MeV)	σ_{Exp} (nb)	$\sigma_{Exp1}/\sigma_{Exp2}$
ER-CE1-CE2 (^{255}No$^{m2\to m1}$)	17.3	12 ± 2	2.4 ± 0.61
	21.3	5.1 ± 1	
^{255}No	17.3	398 ± 50	3.4 ± 0.97
	21.3	117 ± 30	
^{254}No^{m2}	17.3	9.6 ± 3	0.15 ± 0.05
	21.3	64 ± 8	
^{254}No^{m1}	17.3	157 ± 30	0.41 ± 0.09
	21.3	383 ± 50	
^{254}No	17.3	619 ± 60	0.35 ± 0.05
	21.3	1778 ± 200	

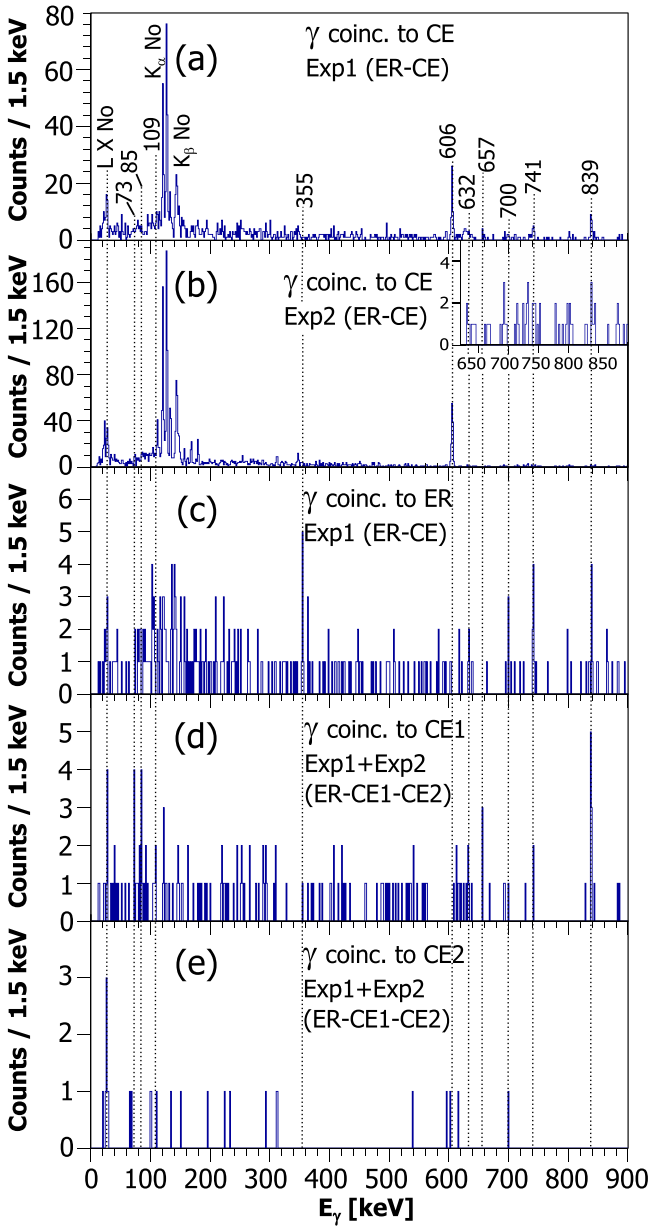

FIG. 2. Energy spectrum of γ transitions in prompt coincidence (see Sec. II) with CEs from ER-CE correlations in (a) Exp1 and (b) Exp2. Inset of (b) shows the energy range 620–900 keV. (c) γ transitions in prompt coincidence with ERs from ER-CE correlations in Exp1. Summed (Exp1 and Exp2) energy spectra of γ transitions in prompt coincidence with (d) CE1 or (e) CE2 from ER-CE1-CE2 correlation chains.

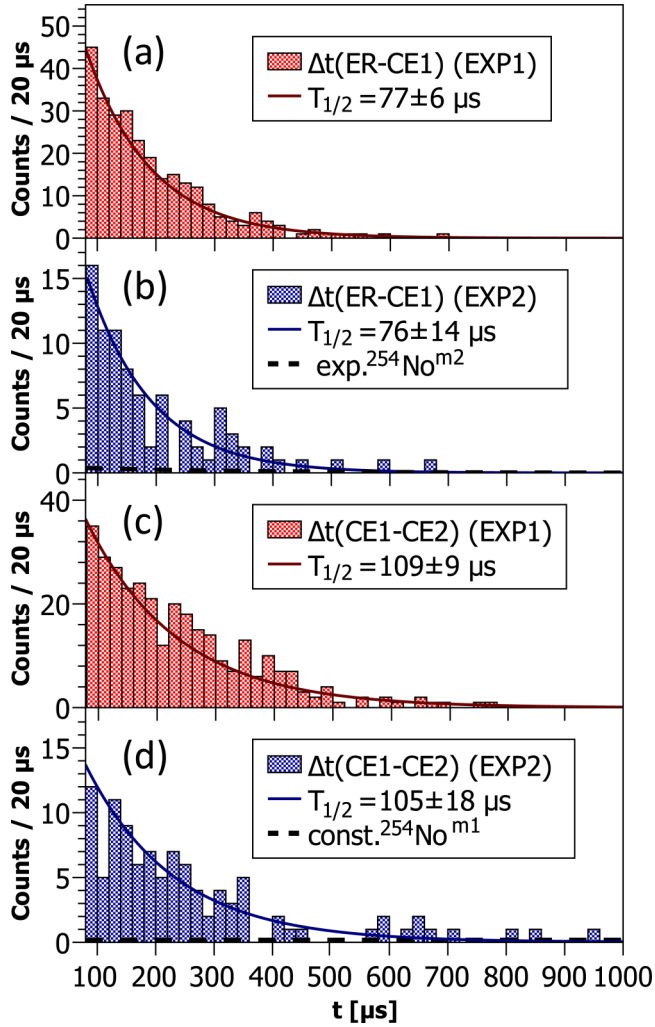

FIG. 3. Time-difference distributions in the range 80–1000 μs between implantation of ER and registration of CE1 in (a) Exp1 (red), (b) Exp2 (blue), or between registration of CE1 and CE2 in (c) Exp1 (red), (d) Exp2 (blue). Solid red and blue lines represent the fits of the data with exponential functions. Dashed black lines denote contributions from ^{254}No^{m2} in (b) and ^{254}No^{m1} in (d), respectively.

with energies 73, 85, 109 keV, and L x rays of nobelium were recorded [Fig. 2(d)]. In coincidence with CE2, only L x rays of nobelium were found [Fig. 2(e)]. No intense K x rays of nobelium, 606-keV or other γ rays originating in the deexcitation of ^{254}No^{m2} were observed in coincidence either with CE1 or CE2. Therefore, we attribute the γ rays (73, 85, 109 keV, etc.) and L x rays of nobelium, found in coincidence with CEs from correlation chains, to the deexcitation of the isomeric state in ^{255}No.

In both experiments, we extracted time-difference [Δt(ER-CE1), Δt(CE1-CE2)] distributions from ER-CE1-CE2 correlation chains (Fig. 3) and applied the fit by exponential function using the maximum likelihood minimization method. As a correction for the $\approx$5% contribution of the ^{254}No isomeric states in these correlation chains in Exp2, another exponential function with ^{254}No^{m2} half-life of 198 μs [12] was added in the fitting of Δt(ER-CE1) distribution [Fig. 3(b)]. For Δt(CE1-CE2) distributions this correction was in the form of a constant function as the ^{254}No^{m1} half-life of 275 $\pm$ 7 ms is more than two orders of magnitude longer than the correlation time of 1 ms [Fig. 3(d)]. The contribution of the ^{254}No isomeric states in Exp1 was negligible (<1%). Resulting half-lives obtained from Exp1 and Exp2 were equal within the uncertainties (Fig. 3) and matched those extracted from ER-CE chains (Exp1) where the coincidence of CEs with 632-, 657-, 741-, or 839-keV γ transitions was required

TABLE IV. Half-lives ($T_{1/2}$) in μs and mean values of CE energies ($\overline{E}_{CE}$) in keV from (a) ER-CE1-CE2 (assigned to ^{255}No; see Table III) and (b) ER-CE correlation chains compared to (c) corresponding values for ^{254}No^{m2} and ^{254}No^{m1}. For the ER-CE sequences, we required a coincidence (see Sec. II) of the 355-, 632-, 657-, 741-, or 839-keV γ ray with either ERs or CEs (denoted in bold).

		(b) ER-CE (Exp1)							
(a) ER-CE1-CE2	(Exp1 | Exp2)	E_γ (keV)	355	632	657	741	839	(c) ^{254}No^{m2,m1}	
$T_{1/2}$(ER-CE1)	$77 \pm 6 \mid 76 \pm 14$	$T_{1/2}$[ER-(**CE-γ**)]	—	75^{+61}_{-23}	82^{+65}_{-26}	79^{+34}_{-18}	79^{+23}_{-15}	$T_{1/2}$[12]	198 ± 13
$\overline{E}_{CE1}$	$258 \pm 10 \mid 263 \pm 10$	$\overline{E}_{CE}$	—	282 ± 34	208 ± 17	249 ± 21	265 ± 16	$\overline{E}_{CE}$	388 ± 10
$T_{1/2}$(CE1-CE2)	$109 \pm 9 \mid 105 \pm 18$	$T_{1/2}$[(**ER-γ**)-CE)]	92^{+62}_{-27}	128^{+310}_{-53}	—	104^{+63}_{-28}	121^{+99}_{-37}	$T_{1/2}$[12]	$2.75 \pm 0.07 \times 10^5$
$\overline{E}_{CE2}$	$208 \pm 10 \mid 203 \pm 10$	$\overline{E}_{CE}$	213 ± 19	258 ± 62	—	204 ± 22	210 ± 20	$\overline{E}_{CE}$	257 ± 10

(Table IV). These half-lives of 77 ± 6 μs and 109 ± 9 μs differ significantly in comparison with corresponding values for ^{254}No isomeric states (see Table IV), and we attribute them to ^{255}No^{m2} and ^{255}No^{m1}, respectively. The order is established by the coincidence behavior with ER for ^{255}No^{m1}

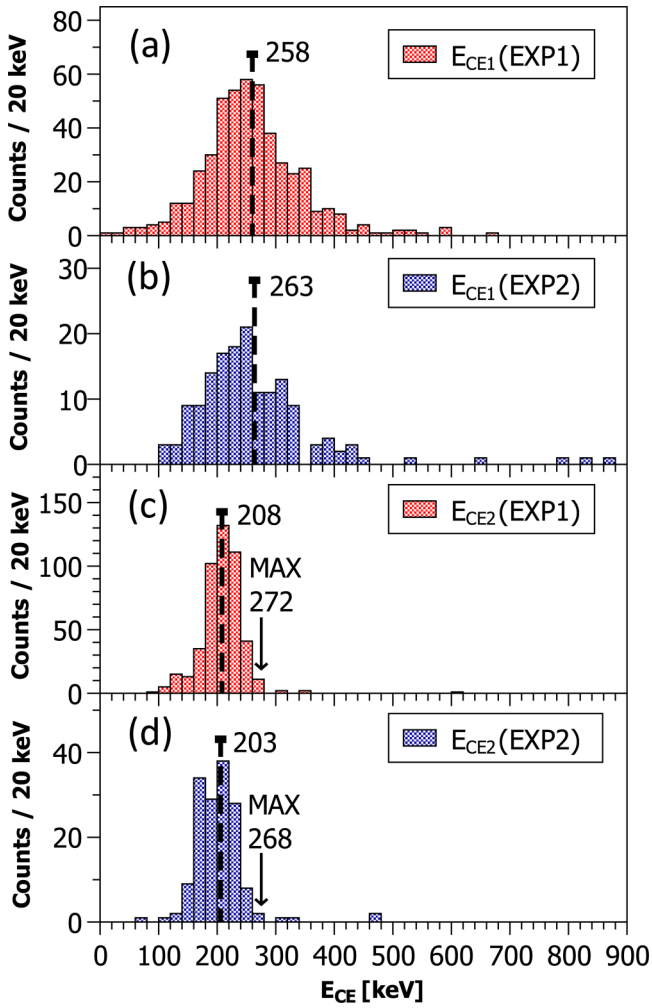

FIG. 4. Energy distribution of CE1 in (a) Exp1 (red), (b) Exp2 (blue), or CE2 in (c) Exp1 (red), (d) Exp2 (blue) from ER-CE1-CE2 correlation chains. The dashed vertical lines denote mean values of the CE energy in keV. An arrow denotes maximum energy in keV.

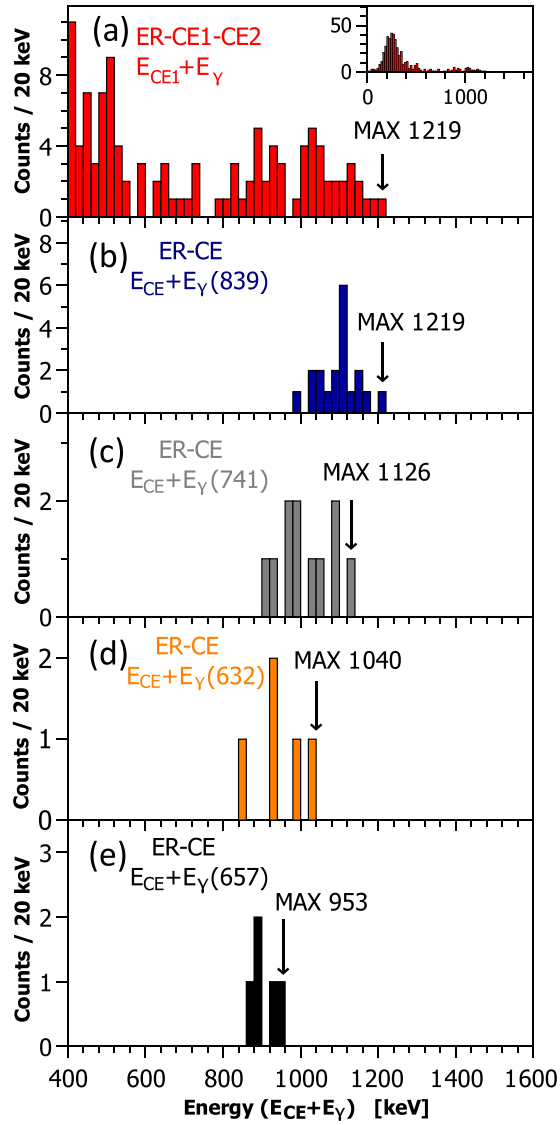

FIG. 5. (a) Energy spectrum of CE1 added to the energy of coincident γ rays from ER-CE1-CE2 correlations in the range 400–1600 keV. Inset of (a) shows the full energy range 0–1750 keV. Energies of CEs from ER-CE correlations summed with coincident (b) 839-, (c) 741-, (d) 632-, or (e) 657-keV γ rays. An arrow denotes the maximum of energy in keV.

and γ rays or CEs for ^{255}No^{m2}, respectively. In order to search for short-lived ($\sim\mu$s) isomeric states, we separately evaluated time differences [Δt(ER-γ) <5 μs] from ER-CE sequences in Exp1 based on TAC (STOP-Ge) values. In this case we required a coincidence of ERs and γ transitions with energies 355-, 632-, 741-, and 839-keV [Fig. 2(c)]. The half-life of these events was established as $1.2^{+0.6}_{-0.4}$ μs and assigned as a third isomeric state, ^{255}No^{m3}. We ruled out the contamination of Δt(ER-CE1) or Δt(CE1-CE2) distributions from ^{255}No^{m3} as its half-life of $1.2^{+0.6}_{-0.4}$ μs is $\approx$20 times shorter than the lower limit of 25 μs for members of correlation chains (see Sec. II).

Signal of decays (e.g., α decay or CEs) in the STOP detector can be summed with the tail of ER signal if they follow shortly (up to $\approx$500 μs) after the implantation of ERs. This pileup effect, which depends on the time difference between the implantation of ER and decay, can create deviation of measured decay energy. To suppress this effect, we applied an energy correction as discussed in Ref. [28]. For higher accuracy, this correction was scaled according to the energy of ERs from correlation chains discussed in this paper. The energy distributions of CE1 or CE2 from ER-CE1-CE2 correlation chains and their mean values were almost identical in both experiments, suggesting their identical origin (Fig. 4). We obtained mean values of the CE energy similar to CE2 from such ER-CE sequences, when the coincidence of ERs with the 355-, 632-, 741-, or 839-keV γ transition was required (Table IV). These values also relatively differ in comparison to energies of CEs attributed to deexcitation of ^{254}No isomeric states. Because of their various CE energies or different half-lives (see Table IV), the ^{254}No isomeric states as the origin of ER-CE1-CE2 correlations can be ruled out.

The lower limit of the ^{255}No^{m2} excitation energy can be roughly estimated as a sum of CE energy and coinciding γ transitions. We added the energies of CE1 from the ER-CE1-CE2 correlation chains and the coincident γ-ray transitions [Fig. 5(a)], whereby a maximum of 1219 keV was obtained. Summing only CEs from ER-CE correlations coincident with the 839-keV γ ray yielded a similar maximum [Fig. 5(b)]. Other transitions with the energies 741, 632, and 657 keV provided lower maxima [Figs. 5(c)–5(e)].

IV. DISCUSSION

A. Decay of ^{255}No^{m1} ($T_{1/2} = 109 \pm 9$ μs)

The narrow distributions of CE2 energies from ER-CE1-CE2 correlations [see Figs. 4(c) and 4(d)] indicate a relatively simple decay path of ^{255}No^{m1}. We roughly estimated the ^{255}No^{m1} excitation energy as 240–300 keV based on the $\approx$270 keV maximum of CE2 energy distributions. The $1/2^+$[620] g.s. configuration of ^{255}No is known from previous studies [8,9] together with the $3/2^+$[622] level ($E^* =$ 147 keV), which promptly decays into members of the g.s. band [11].

Below 700 keV, three "high-spin" Nilsson levels $7/2^+$[613], $9/2^-$[734], and $11/2^-$[725] are predicted for $N = 153$ isotones [3,4]; two of them were also identified as excited levels in neighboring isotopes, i.e., $11/2^-$[725] in ^{253}Fm [29] and ^{257}Rf [30], $7/2^+$[613] in ^{253}Fm [29]. Thus, these "high-spin" Nilsson levels represent candidates for the configuration of ^{255}No^{m1}. However, the $7/2^+$[613] configuration can be excluded. With $E^* \approx 270$ keV it would promptly decay into the $3/2^+$[622] level via $E2$ transition. The $9/2^-$[734] and $11/2^-$[725] levels can populate the $3/2^+$[622] or $7/2^+$[613] state. Decay into the latter can be excluded for the $9/2^-$[734] level as half-lives of $E1$ transitions without any hindrance are several orders of magnitude shorter than the half-life of ^{255}No^{m1}. For decay into the $3/2^+$[622] state only transitions with $\Delta L \geqslant 3$ can be expected. The energies of $E3$ transitions (mostly converted on the L and M shells) are limited to values $\leqslant$ 300 keV due to a maximum of CE2 energies 240–300 keV [Figs. 4(c) and 4(d)] resulting in half-lives above milliseconds according to Weisskopf estimates [31]. However, experimental half-lives are typically even longer, by approximately one order of magnitude, than the Weisskopf estimates [32]. As decays via $E3$ transitions are therefore at least two orders of magnitude longer than the half-life of ^{255}No^{m1}, we excluded this possibility. Because of the positive parity of available single-particle levels, only hindered $E1$ type (e.g., populating members of the rotational band) or $M2$ type are available as first transitions deexciting ^{255}No^{m1} with configurations of $9/2^-$[734] or $11/2^-$[725]. Half-lives of electromagnetic decays can be strongly enhanced in comparison to Weisskopf estimates when the conservation of the total angular momentum projection K is violated. This feature occurs for the transitions with lower multipolarities than the corresponding ΔK, and can be quantified by the hindrance factor F_W as a ratio of experimental half-lives to Weisskopf estimates [32]. Possible ΔK values for electromagnetic transitions with given multipolarities as a function of hindrance factors were summarized by Löbner [32] and Kondev *et al.* [33]. For known initial and final Nilsson configurations, the range of ΔK values for a given transition can consequently limit the variety of deexcitation scenarios. In addition, the absence of nobelium K x rays and no intense γ rays in coincidence with CE2 from ER-CE1-CE2 correlation chains [see Fig. 2(e)] suggests that all transitions in the deexcitation path of ^{255}No^{m1} are highly converted with energies below the K-shell binding energy ($\approx$147 keV [26]).

We estimated ΔK values based on hindrance factors calculated for different energies of available $E1$ or $M2$ transitions and the Löbner systematics. Possible scenarios for deexcitation of ^{255}No^{m1} are summarized in Table V. Deexcitation of ^{255}No^{m1} via $E1$ transition requires low energy (below 25 keV), in order to be strongly converted (ICC($E1$, 25 keV) = 3.6 [34]). Otherwise, we should observe intense γ rays in coincidence with CE2, which is not the case [see Fig. 2(e)]. Moreover, if members of the $3/2^+$[622] rotational band are populated, we could expect $\approx$5 counts of 97-keV and $\approx$4 counts of 147-keV γ rays in Fig. 2(e). Both of these transitions were previously observed in Ref. [11] depopulating the $3/2^+$[622] bandhead. As none of them are present in Fig. 2(e), we ruled out the scenarios leading via the $3/2^+$[622] band. Most likely the deexcitation of ^{255}No^{m1} proceeds via $M2$ transition into the $7/2^+$[613] level or low-energy (below 25 keV) $E1$ transition into members of its rotational band (Table V). Excitation energy of the $7/2^+$[613] level should

TABLE V. Scenarios for deexcitation of ^{255}No^{m1}. The ΔK values for corresponding transitions estimated based on Löbner's systematics and hindrance factors (F_W) are given. Bandhead configurations for populated states are denoted in brackets. Hindrance factors were calculated as the ratio of observed half-life 109 ± 9 μs and Weisskopf estimates.

	E_γ (keV)	F_W	ΔK	Scenario	Bandhead
$E1$	50	1.6×10^8	2, 3	$11/2^-[725] \rightarrow 9/2^+$	$(7/2^+[613])$
				$11/2^-[725] \rightarrow 11/2^+$	$(7/2^+[613])$
				$9/2^-[734] \rightarrow 9/2^+$	$(3/2^+[622])$
				$9/2^-[734] \rightarrow 7/2^+$	$(3/2^+[622])$
$M2$	50	180	2	$11/2^-[725] \rightarrow 7/2^+$	$(7/2^+[613])$
	100	270			

be close above or below the 147 keV (excitation energy of $3/2^+[622]$ state). Otherwise, the $3/2^+[622]$ state would be populated in the deexcitation of the $7/2^+[613]$ level.

Theoretical excitation energies of the $9/2^-[734]$ level in ^{255}No are 470 [3] and 440 keV [4]. For the $11/2^-[725]$ level these energies are 230 [3] and 280 keV [4], respectively. While the former values are somewhat higher, the latter are in good agreement with ^{255}No^{m1} excitation energy of 240–300 keV. The presence of single-particle $11/2^-[725]$ isomeric states in the neighboring isotones ^{253}Fm [29] and ^{257}Rf [35] also supports $11/2^-[725]$ as the configuration of ^{255}No^{m1}. In addition, population of members of its rotational band from ^{255}No^{m2} or ^{255}No^{m3} should be favored over members of the $9/2^-[734]$ band due to the lower ΔK value. Therefore, we tentatively assign the Nilsson configuration of $11/2^-[725]$ to ^{255}No^{m1}.

B. Decay of ^{255}No^{m2} ($T_{1/2} = 77 \pm 6$ μs)

An isomeric state in ^{255}No was previously tentatively suggested on the basis of the 741- and 839-keV γ transition half-lives of 105 ± 25 and 130 ± 25 μs, respectively, in Ref. [12]. These high-energy γ rays were observed in coincidence with CEs correlated to ERs. Our results indicate a somewhat lower but still compatible value of $T_{1/2} = 77 \pm 6$ μs and $T_{1/2} = 76 \pm 14$ μs derived from time differences of ER-CE1-CE2 correlations in Exp1 and Exp2 [Figs. 3(a) and 3(b)]. These half-lives were in good agreement with half-lives of individual γ lines with energies 632, 657, 741, and 839 keV extracted from ER-CE correlation chains in Exp1 (see Table IV).

The wide energy distribution of CE1 from ER-CE1-CE2 sequences [Figs. 4(a) and 4(b)] suggests cascades of highly converted transitions as a part of the ^{255}No^{m2} deexcitation path. We observed 73-, 85-, and 109-keV transitions [Fig. 2(d)] and tentatively interpret these γ rays as members of the $11/2^-[725]$ band based on the previously assigned configuration of ^{255}No^{m1}. Similar transitions $13/2^- \xrightarrow{73\text{ keV}} 11/2^-$, $15/2^- \xrightarrow{86\text{ keV}} 13/2^-$, and $19/2^- \xrightarrow{112\text{ keV}} 17/2^-$ of the same type of high-spin band were observed in ^{257}Rf [35]. Additionally, energy differences of 98 and 109 keV derived from the 839-, 741-, and 632-keV γ rays fit the energy of $17/2^- \rightarrow 15/2^-$ and $19/2^- \rightarrow 17/2^-$ transitions in the analogous band in ^{257}Rf [35]. However, according to a more recent study of ^{257}Rf, the first member of the $11/2^-[725]$ rotational band is an 86-keV transition [36]. Thus, we suggest a two different scenarios for population of three consecutive members of the $11/2^-[725]$ band via 632-, 741-, and 839-keV transitions. In the first scenario, the first member of the $11/2^-[725]$ band is a 73-keV transition and populated levels are $19/2^-$, $17/2^-$, and $15/2^-$. In the second scenario the $17/2^-$, $15/2^-$, $13/2^-$ levels are populated and the first transition has an energy of 85 keV. These two scenarios are included in all following discussions and in the ^{255}No decay scheme proposed in Sec. IV D.

TABLE VI. Possible ΔK values for transitions deexciting ^{255}No^{m2} estimated based on Löbner's systematics and hindrance factors (F_W). The hindrance factors were calculated as the ratio of the observed half-life of 77 ± 6 μs to Weisskopf estimates.

Transition	E_γ (keV)	F_W	ΔK Löbner est.
$M1$	50	4.3×10^7	3 or 4
	100	4.8×10^7	3 or 4
	150	7.6×10^7	4
$E2$	50	3.4×10^3	2, 3, or 4
	100	4.4×10^3	2, 3, or 4
	150	6.0×10^3	2, 3, or 4
$M2$	50	1.3×10^2	2
	100	1.9×10^2	2
	150	2.7×10^2	2

The 632-, 741-, and 839-keV γ lines were observed also in coincidence [Δt(ER-γ) <5 μs] with ERs [Fig. 2(c)]. This observation indicates that these γ rays are stemming from an intermediate level, which is fed both by ^{255}No^{m2} and yet another isomer with a very short half-life (see Sec. IV C). Transitions feeding this intermediate level from ^{255}No^{m2} should be mostly converted on the -shell as no intense γ rays (except for 632, 657, 741, and 839 keV) and only very weak K x rays of nobelium were registered in coincidence with CE1 [Fig. 2(d)]. The $E1$ character of these transitions can be excluded based on its low internal conversion coefficient (ICC($E1$, 25 keV) = 3.6 [34]) and lack of intense low-energy γ rays [see Fig. 2(d)]. We calculated ΔK values for a different type of transition ($E_\gamma < 150$ keV) based on their hindrance factors and Löbner's systematics [32]. All possible ΔK values are in the range 2–4 (Table VI).

We can derive the character of the γ lines with energies of 632, 741, and 839 keV. The possibility of all three transitions having multipolarity $L = 2$ can be ruled out, as they are emitted from the same level and populate three consecutive states in a rotational band [see Fig. 6(a)]. At least two of them should have multipolarity $L = 1$. Because of their similar energies and intensities, the scenario with three dipole transitions being either $E1$ or $M1$ type is the most probable. The electromagnetic character of these high-energy γ rays can be determined based on their K x ray yields, related to the transition's internal conversion. If these γ lines are of $M1$ type, we could expect, considering Ge-detector efficiency, ≈16 counts of K x rays in coincidence with CE1 (Table VII) from Exp1 alone, contrary

TABLE VII. Expected yields of K x rays (N_K) and following CE1 with energy $E > 600$ keV (N_{CE}) from deexcitation of the 632-, 741-, and 839-keV γ transitions via internal conversion. Yields were calculated for ER-CE1-CE2 correlation chains in Exp1. The probability of CE depositing full energy was estimated using the GEANT4 simulation toolkit [38].

E_γ (keV)	$N_K(E1)$	$N_K(M1)$	$N_K(E2)$	$N_K(M2)$	$N_{CE}(E1)$	$N_{CE}(M1)$	$N_{CE}(E2)$	$N_{CE}(M2)$
632	0.1	3.5	0.4	7.1	0.2	4.1	0.6	8.7
741	0.3	5.7	0.8	11.6	0.2	3.4	0.5	7.1
839	0.4	6.8	1.1	13.9	0.1	2.1	0.4	4.5
$\sum$	0.8	16.0	2.3	32.6	0.5	9.6	1.5	20.3

to 4 ± 2 counts, which were observed in added data from both experiments [see Fig. 2(d)]. On the other hand, their $E1$ type would yield a more compatible value of ≈ 1 K x rays (see Table VII). Another useful quantity is the yield of electrons with energies $\geqslant 500$ keV from the internal conversion of the 632-, 741-, and 839-keV γ transitions. As a result of the long range of >500 keV electrons (>1 mm in Si [37]) compared to the thickness of the STOP detector of 0.3 mm, only a fraction of these electrons will deposit their full energy. Using the GEANT4 simulation toolkit [38], we estimated this fraction from the internal conversion of these γ transitions, depositing their full energy in the STOP detector (Table VII). Nevertheless, the energies of these CEs will be summed with the energies of CEs from the deexcitation of the other converted transitions (e.g., 73, 85, 98, and 109 keV) in the cascade, leading to an energy minimum of 600 keV. Assuming their $M1$ or $E1$ type, we expect ≈ 10 or ≈ 1 counts of CE1 ($E_{CE1} \geqslant 600$ keV), respectively, from the ER-CE1-CE2 correlation events in Exp1. The latter value of ≈ 1 is in agreement with the 1 count observed for CE1 [see Fig. 4(a)]. Therefore, based on the K x ray and CE1 ($E_{CE1} \geqslant 600$ keV) yields of the 632-, 741-, and 839-keV γ transitions, we tentatively assign $E1$ as their character and $I^\pi = 15/2^+, 17/2^+$ to the intermediate level, which they depopulate. We estimate excitation energy of the $(15/2^+, 17/2^+)$ level as 1150–1300 keV by adding together the 839-keV transition, 240–300 keV as the excitation energy of ^{255}No^{m1}, and the 85- or 73- and 85-keV transitions (members of the $11/2^-$[725] rotational band; see Fig. 6(a) and Sec. IV B).

The 657-keV γ ray is only in coincidence with CE1 [and not with ERs; see Fig. 2(d) and Table IV], therefore it does not stem from the $17/2^+$ intermediate level. Presumably it directly deexcites ^{255}No^{m2}, since a different deexcitation path would require another high-spin intermediate level in addition to the $(15/2^+, 17/2^+)$ state. To evaluate the spin of ^{255}No^{m2} we estimated ΔK values for different types of 657-keV γ transition based on calculated hindrance factors and Löbner's systematics [32]. All possible ΔK values are in the range of 4–6 (Table VIII). As K-isomeric states tend to have the highest possible spin [12], the K value of ^{255}No^{m2} can be estimated as the sum of ΔK of the deexciting transition and the K value of the populated state. The $K = 19/2$–$25/2$ values were obtained in case of the low-energy transitions ($\Delta K = 2$–4) populating a member of the $(15/2^+, 17/2^+)$ rotational band. Similarly, we derived values of $K = 19/2$–$23/2$ for the 657-keV γ transition ($\Delta K = 4$–6) leading to a member of the $11/2^-$ band. Therefore, we tentatively assign $K = 19/2, 21/2,$ or $23/2$ for ^{255}No^{m2} as the overlap of these two ranges and denote it as presumably a three-quasiparticle (3-qp) K isomer (see Sec. IV D).

The excitation energy of ^{255}No^{m2} can be roughly estimated based on the maximum of the summed energies of CE1s and coincident γ rays [see Figs. 5(a) and 5(b)]. Therefore, we estimated the ^{255}No^{m2} excitation energy as 1400–1600 keV by adding together 1160–1280 keV as the maximum of the summed energies of the CE1s and coincident γ rays [see Fig. 5(a) and 5(b)], and 240–300 keV as the excitation energy of ^{255}No^{m1}. Because of the presumably higher number of cascade transitions in the decay path of ^{255}No^{m2} in comparison to ^{255}No^{m1}, we used a larger interval of 1160–1280 keV for the estimate of the maximum of the summed energies of the CE1s and coincident γ rays.

C. Decay of ^{255}No^{m3} ($T_{1/2} = 1.2^{+0.6}_{-0.4}$ μs)

The presence of fourteen 632-, 741-, 839-keV γ rays in coincidence with the implanted ERs [Fig. 2(c)] cannot be explained via decay of ^{255}No^{m2}. In that case, only 1^{+2}_{-1} coincidence events are expected because of the much longer half-life of ^{255}No^{m2} than the coincidence time. This large difference indicates that another isomeric state, feeding the intermediate level, must be populated in the reaction. The half-life of ^{255}No^{m3} should be $\gtrsim 1$ μs to survive the flight through the separator. Indeed, we obtained a half-life of $T_{1/2} = 1.2^{+0.6}_{-0.4}$ μs based on the TAC (STOP-Ge) values of the 355-, 632-, 741-, and 839-keV γ transitions found in coincidence with ER from ER-CE correlation chains (see Sec. III). The decay path of ^{255}No^{m3} proceeds via the 632-, 741-, and 839-keV transitions

TABLE VIII. Possible ΔK values for the 657-keV γ transition deexciting ^{255}No^{m2} estimated on the basis of Löbner systematics and calculated hindrance factors (F_W). The hindrance factors were calculated as the ratio of partial half-life of the 657-keV γ transition ≈ 540 μs and corresponding Weisskopf estimates. In the calculation of the 657-keV γ transition partial half-life, the ratio of the 657-keV and the sum of the 632-, 657-, 741-, and 839-keV γ transition intensities ($\approx 1/7$) was included.

Transition	E_γ (keV)	F_W	ΔK Löbner est.
$E1$	657	9.3×10^{11}	5 or 6
$M1$		8.8×10^{9}	5 or 6
$E2$		1.2×10^{7}	4 or 5
$M2$		1.4×10^{5}	4 or 5

and feeds ^{255}No^{m1}. Such a decay path is supported by the excellent agreement of half-lives [Δt((ER-γ)-CE)] extracted from ER-CE sequences with the half-life of ^{255}No^{m1} based on ER-CE1-CE2 correlation chains. In addition, mean values of the CE energy from these ER-CE chains are in good accord with CE1 attributed to deexcitation of ^{255}No^{m1} (see Table IV).

We assign the 355-keV γ line to the decay scheme of ^{255}No^{m3} as it was observed only in coincidence with ERs [Fig. 2(c)]. Otherwise, it should be present also in coincidence with CE1 from ER-CE1-CE2 correlations, which is not the case [see Fig. 2(d)]. However, it cannot be unambiguously attributed to the decay of the ^{255}No^{m3} and its placement in the decay scheme is only tentative [see Fig. 6(a)]. Consequently, we estimate a lower limit of the ^{255}No^{m3} excitation energy as $\geqslant$ 1500 keV being the sum of the (15/2$^+$, 17/2$^+$) level excitation energy 1150–1300 keV and the 355-keV transition. We denote ^{255}No^{m3} as a 3-qp K isomer based on its excitation energy, similar to known K-isomeric states in neighboring isotopes with $E^* > 1000$ keV (see, e.g., [28,36,39,40]). ^{255}No^{m3} populates the (15/2$^+$, 17/2$^+$) level or members of its rotational band with a half-life of $1.2^{+0.6}_{-0.4}$ μs. Such a half-life can be achieved either by the $\Delta K \geqslant 2$ hindrance for $L = 1$ transitions [32] or via transitions with $L = 2$ according to Weisskopf estimates [31]. Therefore, we tentatively assign $I \geqslant 19/2$ for ^{255}No^{m3}. No additional information about the spin or parity of this isomeric state can be extracted from our data.

D. Decay scheme of ^{255}No

Based on the analysis above, we propose a tentative decay scheme of ^{255}No in Fig. 6(a). Neighboring isotone ^{257}Rf shares a similarity with ^{255}No in the deexcitation of high-K isomer, as shown in Fig. 6(b). For ^{257}Rf, feeding the members of the rotational band built on the low-energy ($E^* = 70$ keV) single-particle isomeric state 11/2$^-$[725] via an $E1$ transition from a high-energy, high-K, 3-qp isomer was suggested [36]. For heavy $N = 151$ isotones, a systematics of short-lived low-energy isomeric states with Nilsson configuration 5/2$^+$[622] was found. However, high-K isomeric states identified in ^{255}Rf and ^{253}No populate only rotational members of the g.s. band. In ^{255}Rf, two high-energy (900–1450 keV) presumably K-isomeric states are feeding one another and also the g.s. band with the Nilsson configuration 9/2$^-$[734] [28]. In ^{253}No the g.s. band is fed from a K-isomeric state with excitation energy $\lesssim$ 1380 keV [40]. A summary of the properties for these high-K isomeric states with their tentative 3-qp configurations is given in Table IX.

Energies of possible 3-qp configurations were previously calculated for ^{257}Rf [36] using the axially deformed Woods-Saxon potential with the set of universal parameters [41] for the single-particle orbitals and the Lipkin-Nogami approach [42] with the average gap method [43] for pairing correlations. The total energy of a state was achieved with the standard liquid-drop model [44] and Strutinsky-shell correction with blocking effects. Five of these 3-qp configurations have $K = 19/2$, $K = 21/2$, or $K = 23/2$, which we also suggest for ^{255}No^{m2}, all formed by coupling of the two-quasiproton (π^2) or two-quasineutron (ν^2) configuration to

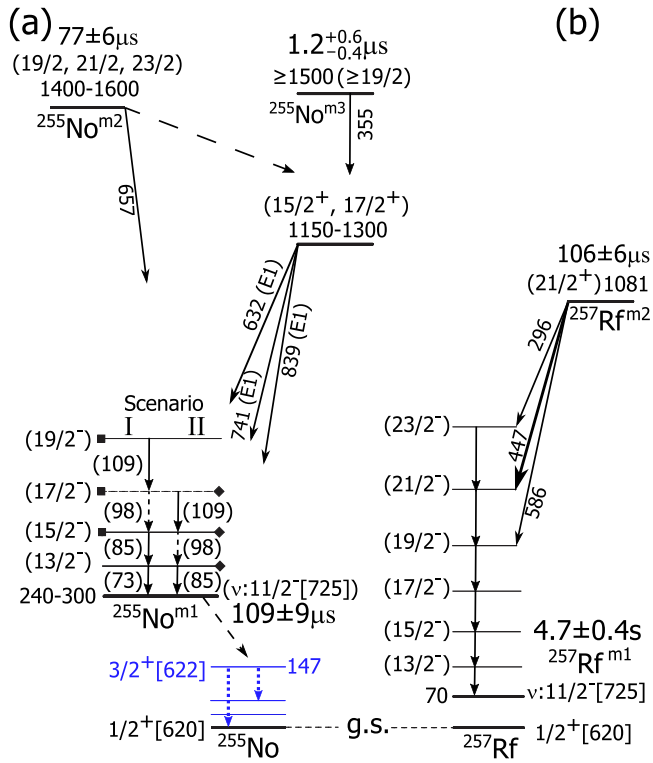

FIG. 6. (a) Tentative decay scheme of isomeric states in ^{255}No. Blue dotted lines represent previously observed levels and transitions [11]. Dashed lines indicate only tentative assignments. Roman numerals and rectangles at the end of horizontal lines correspond to different scenarios where various members of the 11/2$^-$[725] rotational band are populated via 632-, 741-, and 839-keV transitions (see Sec. IV B). (b) Decay scheme of the isotonic neighbor ^{257}Rf [36]. Energies are in keV.

the ν 11/2$^-$[725] single-particle state. It is not possible to pinpoint the 3-qp configuration of ^{255}No^{m2} based on these calculations alone. A deformed neutron shell gap is expected at $N = 152$ [45]. The 3-qp configurations formed from only

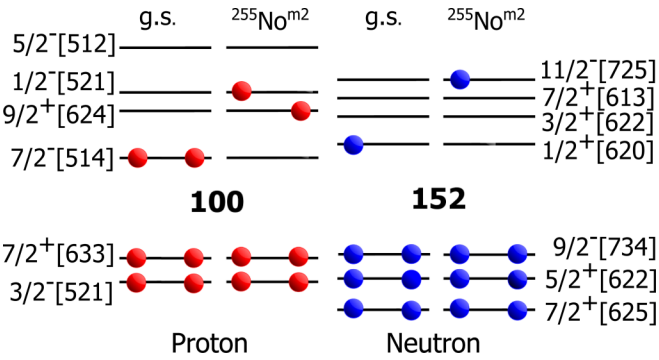

FIG. 7. Ground-state configuration of ^{255}No and tentative ^{255}No^{m2} 3-qp configuration. Given single-particle levels for protons and neutrons were calculated in Ref. [46] with nuclear deformations taken from Ref. [47]. The neutron Nilsson levels 1/2$^+$[620], 3/2$^+$[622], and 5/2$^+$[622] were placed based on the experimental results from Refs. [8,9], [11], and [5], respectively.

TABLE IX. Spin-parity assignments, excitation energies (E^*), half-lives ($T_{1/2}$), and tentative Nilsson configurations of high-K 3-qp isomeric states in $N = 151$ and $N = 153$ isotopes.

Nucleus	I^π	E^* (keV)	$T_{1/2}$ (μs)	Tentative configuration (p-p-n)	Reference
^{253}No	$(25/2^+)$	$\lessapprox$ 1380	706 ± 24	$7/2^-[514] \otimes 9/2^+[624] \otimes 9/2^-[734]$	[40]
^{255}Rf	$(\geqslant 19/2)$	900–1200	15^{+6}_{-4}	$1/2^-[521] \otimes 9/2^+[624] \otimes 9/2^-[734]$	[28]
^{255}Rf	$(\geqslant 19/2)$	1150–1450	38^{+12}_{-7}	—	[28]
^{255}No	(19/2, 21/2, 23/2)	1400–1600	77 ± 6	$1/2^-[521] \otimes 9/2^+[624] \otimes 11/2^-[725]$	This work
^{255}No	$(\geqslant 19/2)$	$\geqslant$ 1500	$1.2^{+0.6}_{-0.4}$	—	This work
^{257}Rf	$(21/2^+)$	1081	106 ± 6	$1/2^-[521] \otimes 9/2^+[624] \otimes 11/2^-[725]$	[36]

unpaired neutrons require a neutron to be excited across this gap (see Fig. 7). Therefore, the excitation energies of $\nu^2 \otimes \nu\, 11/2^-[725]$ 3-qp states will then be higher in comparison to $\pi^2 \otimes \nu\, 11/2^-[725]$ 3-qp states which do not require excitation across a shell gap. Thus, coupling of two-quasiproton configurations with the $\nu\, 11/2^-[725]$ level is favored. The 3-qp configuration with the lowest excitation energy and $K = 19/2$, $K = 21/2$, or $K = 23/2$, which consists of a proton pair and $\nu\, 11/2^-[725]$, is $1/2^-[521] \otimes 9/2^+[624] \otimes 11/2^-[725]$ (see Fig. 7 and Table IX). However, as calculations of 2-qp states excitation energies can differ significantly (see, e.g., Refs. [48–50]), other 3-qp configurations of ^{255}No^{m2} are possible. Some additional assumptions can be made for the deexcitation of ^{255}No^{m2}. Its decay path should proceed via the lowest possible ΔK, and it should preferentially not involve a change of the unpaired neutron $11/2^-[725]$. The 3-qp configuration of the $(15/2^+, 17/2^+)$ state being preferably populated from ^{255}No^{m2} should include this neutron configuration. Nevertheless, further experimental data are needed to determine the exact 3-qp configuration of ^{255}No^{m2}.

E. Quasiparticle level systematics of $N = 153$ isotones

Experimental and theoretical single-particle level energies in $N = 153$ isotones are presented in Figs. 8(a)–8(e) [51]. We added the assignment of the $11/2^-[725]$ state in ^{255}No from this work. Clearly, the excitation energy of $11/2^-[725]$ state decreases from ^{253}Fm to ^{255}No, being in line with the

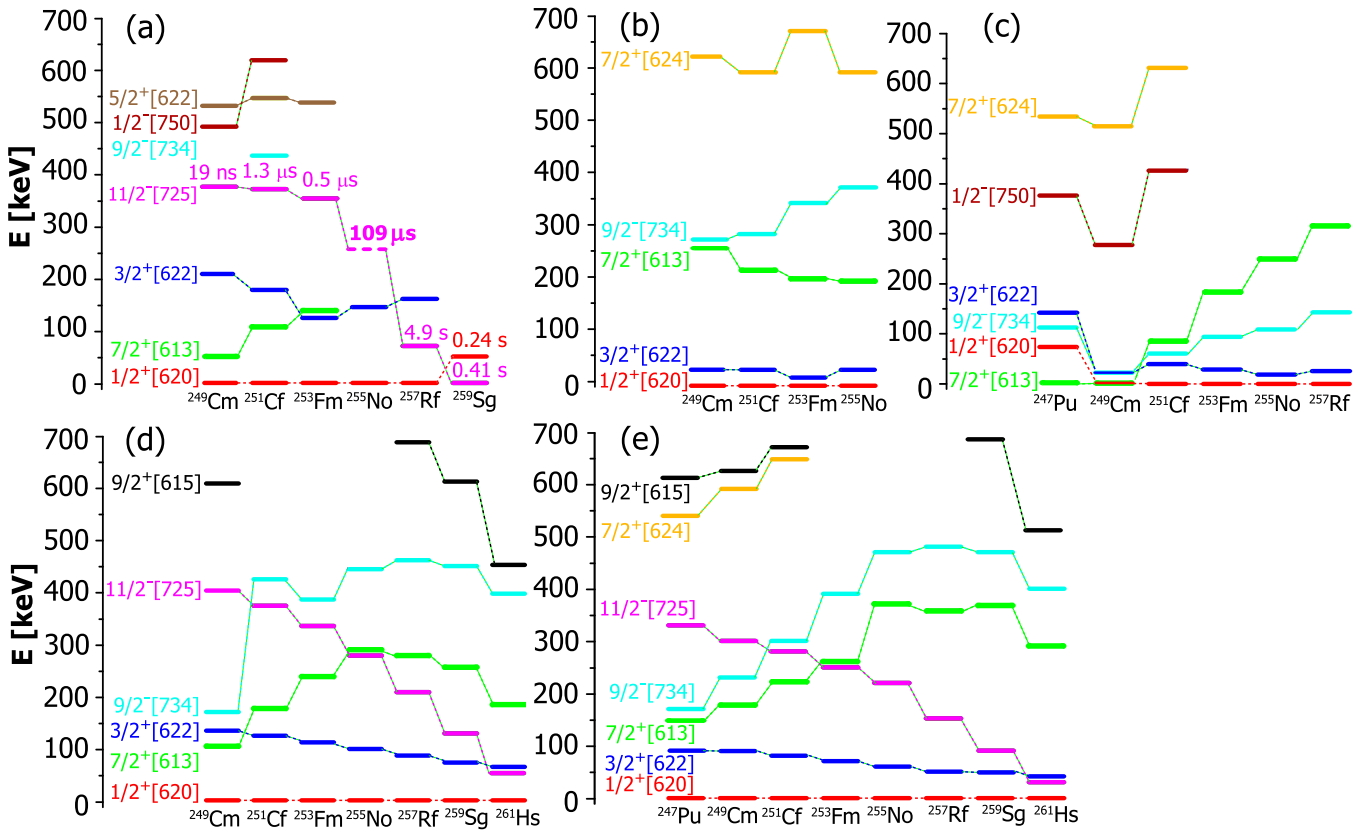

FIG. 8. (a) Experimental single-particle level systematics of $N = 153$ isotones. Theoretical calculations of single-particle levels based on self-consistent models (b) [1] and (c) [2] or macroscopic-microscopic models (d) [4] and (e) [3] are given for comparison. Dashed horizontal line denotes the excitation energy for the $11/2^-[725]$ level (240–300 keV) in ^{255}No assigned in this work.

theoretical predictions of mac-mic models, although followed by a more steep decrease to ^{257}Rf [see Figs. 8(d) and 8(e)]. It has to be noted that self-consistent models are not predicting the $11/2^-$[725] level in the range 0–700 keV [Figs. 8(b) and 8(c)].

V. CONCLUSIONS

The technique of CE correlation was applied to the study of excited states in ^{255}No. We studied three isomeric states in ^{255}No; two of them were identified for the first time. In the case of ^{255}No^{m1}, we estimated its range of excitation energy as 240–300 keV and assigned tentatively the $11/2^-$[725] Nilsson configuration, partially based on $N = 153$ experimental systematics. Such assignment is in agreement with theoretical calculations of quasi-particle level systematics [3,4]. The monotonic decrease of the $11/2^-$[725] level energy from ^{253}Fm to ^{257}Rf was confirmed. For the previously tentatively assigned isomeric state (in the present paper denoted as ^{255}No^{m2}), an improved half-life value of 77 ± 6 μs, a range of excitation energy 1400–1600 keV, and possible spins of $I = 19/2$, $21/2$, and $23/2$ were extracted. Regarding ^{255}No^{m3}, a half-life of $1.2^{+0.6}_{-0.4}$ μs was measured, and lower limits of $E^* > 1500$ keV and $I \geqslant 19/2$ were proposed for its excitation energy and spin, respectively. Concerning ^{255}No^{m2} and ^{255}No^{m3}, both were assigned as K-isomeric states and are an important addition to the systematics of high-K, high-energy isomers in the transfermium region.

ACKNOWLEDGMENTS

We thank the UNILAC staff and the ion source crew for delivering beams of high and stable intensity. We are also grateful to J. Steiner, B. Lommel, and B. Kindler for the production of the large area targets. We want to express our gratitude to H. G. Burkhard and H. J. Schött for the skillful maintenance of the mechanical and electrical components of SHIP. Four of us, A.B., B.A., S.A., and M.V., were supported by the Slovak Research and Development Agency (Contracts No. APVV-18-0268 and No. APVV-20-0532) and by the Slovak grant agency VEGA (Contracts No. 1/0651/21 and No. 2/0067/21). M.V. acknowledges funding from the ESET Foundation, Slovakia.

[1] Z.-H. Zhang, X.-T. He, J.-Y. Zeng, E.-G. Zhao, and S.-G. Zhou, Phys. Rev. C **85**, 014324 (2012).
[2] M. Bender, P. Bonche, T. Duguet, and P.-H. Heenen, Nucl. Phys. A **723**, 354 (2003).
[3] A. Parkhomenko and A. Sobiczewski, Acta Phys. Pol. B **36**, 3115 (2005).
[4] S. Ćwiok, S. Hofmann, and W. Nazarewicz, Nucl. Phys. A **573**, 356 (1994).
[5] S. Antalic, F. P. Heßberger, D. Ackermann, S. Heinz, S. Hofmann, B. Kindler, J. Khuyagbaatar, B. Lommel, and R. Mann, Eur. Phys. J. A **51**, 41 (2015).
[6] A. Sobiczewski, I. Muntian, and Z. Patyk, Phys. Rev. C **63**, 034306 (2001).
[7] A. Ghiorso, T. Sikkeland, and M. Nurmia, Phys. Rev. Lett. **18**, 401 (1967).
[8] F. P. Heßberger, S. Hofmann, D. Ackermann, S. Antalic, B. Kindler, I. Kojouharov, P. Kuusiniemi, M. Leino, B. Lommel, R. Mann, K. Nishio, A. G.Popeko, B. Sulignano, S. Saro, B. Streicher, M. Venhart, and A. V. Yeremin, Eur. Phys. J. A **29**, 165 (2006).
[9] M. Asai, K. Tsukada, H. Haba, Y. Ishii, T. Ichikawa, A. Toyoshima, T. Ishii, Y. Nagame, I. Nishinaka, Y. Kojima, and K. Sueki, Phys. Rev. C **83**, 014315 (2011).
[10] K. Rezynkina, A. Lopez-Martens, K. Hauschild, I. Deloncle, S. Péru, P. Brionnet, M. L. Chelnokov, V. I. Chepigin, O. Dorvaux, F. Déchery, H. Faure, B. Gall, A. V. Isaev, I. N. Izosimov, D. E. Katrasev, A. N. Kuznetsov, A. A. Kuznetsova, O. N. Malyshev, A. G. Popeko, Y. A. Popov, E. A. Sokol, A. I. Svirikhin, and A. V. Yeremin, Phys. Rev. C **97**, 054332 (2018).
[11] M. Asai, K. Tsukada, Y. Kasamatsu, T. K. Sato, A. Toyoshima, Y. Ishii, R. Takahashi, Y. Nagame, T. Ishii, I. Nishinaka, D. Kaji, K. Morimoto, and Y. Kojima, *JAEA Review 2009-36*, JAEA Review Vol. 2009 (JAEA, Tokai, Ibaraki, Japan, 2009), p. 37, JAEA-Tokai Tandem Annual Report.
[12] F. P. Heßberger, S. Antalic, B. Sulignano, D. Ackermann, S. Heinz, S. Hofmann, B. Kindler, J. Khuyagbaatar, I. Kojouharov, P. Kuusiniemi, M. Leino, B. Lommel, R. Mann, K. Nishio, A. Popeko, S. Saro, B. Streicher, J. Uusitalo, M. Venhart, and A. Yeremin, Eur. Phys. J. A **43**, 55 (2010).
[13] S. Antalic, F. P. Heßberger, S. Hofmann, D. Ackermann, S. Heinz, B. Kindler, I. Kojouharov, P. Kuusiniemi, M. Leino, B. Lommel, R. Mann, K. Nishio, S. Saro, B. Streicher, B. Sulignano, and M. Venhart, Eur. Phys. J. A **38**, 219 (2008).
[14] G. Münzenberg, W. Faust, S. Hofmann, P. Armbruster, K. Güttner, and H. Ewald, Nucl. Instrum. Methods **161**, 65 (1979).
[15] S. Hofmann and G. Münzenberg, Rev. Mod. Phys. **72**, 733 (2000).
[16] M. Kaspar and J. Gerl, *GSI Report 1998-1*, 53534, GSI Report Vol. 1998-1 (GSI, Darmstadt, Germany, 1998), p. 195, Wissenschaftlicher Ergebnisbericht der GSI, GSI Annual Report.
[17] F. P. Heßberger, S. Hofmann, I. Kojouharov, and D. Ackermann, Eur. Phys. J. A **22**, 253 (2004).
[18] G. Jones, Nucl. Instrum. Methods Phys. Res., Sect. A **488**, 471 (2002).
[19] W. Bambynek, B. Crasemann, R. W. Fink, H. U. Freund, H. Mark, C. D. Swift, R. E. Price, and P. V. Rao, Rev. Mod. Phys. **44**, 716 (1972).
[20] M. O. Krause, J. Phys. Chem. Ref. Data **8**, 307 (1979).
[21] S. Hofmann, W. Faust, G. Münzenberg, W. Reisdorf, P. Armbruster, K. Güttner, and H. Ewald, Z. Phys. A **291**, 53 (1979).
[22] K. Schmidt, C. Sahm, K. Pielenz, and H. Clerc, Z. Phys. A **316**, 19 (1984).
[23] G. Henning, T. L. Khoo, A. Lopez-Martens, D. Seweryniak, M. Alcorta, M. Asai, B. B. Back, P. F. Bertone, D. Boilley, M. P. Carpenter, C. J. Chiara, P. Chowdhury, B. Gall, P. T. Greenlees, G. Gürdal, K. Hauschild, A. Heinz, C. R. Hoffman, R. V. F. Janssens, A. V. Karpov *et al.*, Phys. Rev. Lett. **113**, 262505 (2014).
[24] M. S. Tezekbayeva, A. V. Yeremin, A. I. Svirikhin, A. Lopez-Martens, M. L. Chelnokov, V. I. Chepigin, A. V. Isaev, I. N. Izosimov, A. V. Karpov, A. A. Kuznetsova, O. N. Malyshev,

R. S. Mukhin, A. G. Popeko, Y. A. Popov, V. A. Rachkov, B. S. Sailaubekov, E. A. Sokol, K. Hauschild, H. Jacob, R. Chakma, O. Dorvaux *et al.*, Eur. Phys. J. A **58**, 52 (2022).
[25] W. Reisdorf and M. Schädel, Z. Phys. **343**, 47 (1992).
[26] C. Thierfelder, P. Schwerdtfeger, F. P. Heßberger, and S. Hofmann, Eur. Phys. J. A **36**, 227 (2008).
[27] R. B. Firestone, in *Table of Isotopes*, 8th ed. (John Wiley and Sons, New York, 1996), Vol. 1, p. 14133.
[28] P. Mosat, F. P. Heßberger, S. Antalic, D. Ackermann, B. Andel, M. Block, S. Hofmann, Z. Kalaninova, B. Kindler, M. Laatiaoui, B. Lommel, A. K. Mistry, J. Piot, and M. Vostinar, Phys. Rev. C **101**, 034310 (2020).
[29] S. Antalic, F. P. Heßberger, D. Ackermann, S. Heinz, S. Hofmann, Z. Kalaninová, B. Kindler, I. Kojouharov, P. Kuusiniemi, M. Leino, B. Lommel, R. Mann, K. Nishio, S. Sáro, B. Streicher, B. Sulignano, and M. Venhart, Eur. Phys. J. A **47**, 62 (2011).
[30] J. Qian, A. Heinz, T. L. Khoo, R. V. F. Janssens, D. Peterson, D. Seweryniak, I. Ahmad, M. Asai, B. B. Back, M. P. Carpenter, A. B. Garnsworthy, J. P. Greene, A. A. Hecht, C. L. Jiang, F. G. Kondev, T. Lauritsen, C. J. Lister, A. Robinson, G. Savard, R. Scott, R. Vondrasek, X. Wang, R. Winkler, and S. Zhu, Phys. Rev. C **79**, 064319 (2009).
[31] V. Weisskopf, Phys. Rev. **83**, 1073 (1951).
[32] K. Löbner, Phys. Lett. B **26**, 369 (1968).
[33] F. Kondev, G. Dracoulis, and T. Kibédi, At. Data Nucl. Data Tables **103-104**, 50 (2015).
[34] T. Kibédi, T. W. Burrows, M. B. Trzhaskovskaya, P. M. Davidson, and C. W. Nestor, Jr., Nucl. Instrum. Methods Phys. Res., Sect. A **589**, 202 (2008).
[35] J. S. Berryman, R. M. Clark, K. E. Gregorich, J. M. Allmond, D. L. Bleuel, M. Cromaz, I. Dragojević, J. Dvorak, P. A. Ellison, P. Fallon, M. A. Garcia, S. Gros, I. Y. Lee, A. O. Macchiavelli, H. Nitsche, S. Paschalis, M. Petri, J. Qian, M. A. Stoyer, and M. Wiedeking, Phys. Rev. C **81**, 064325 (2010).
[36] J. Rissanen, R. M. Clark, K. E. Gregorich, J. M. Gates, C. M. Campbell, H. L. Crawford, M. Cromaz, N. E. Esker, P. Fallon, U. Forsberg, O. Gothe, I.-Y. Lee, H. L. Liu, A. O. Machiavelli, P. Mudder, H. Nitsche, G. Pang, A. Rice, D. Rudolph, M. A. Stoyer, A. Wiens, and F. R. Xu, Phys. Rev. C **88**, 044313 (2013).
[37] L. Pages, E. Bertel, H. Joffre, and L. Sklavenitis, At. Data Nucl. Data Tables **4**, 1 (1972).
[38] S. Agostinelli, J. Allison, K. Amako, J. Apostolakis, H. Araujo, P. Arce, M. Asai, D. Axen, S. Banerjee, G. Barrand, F. Behner, L. Bellagamba, J. Boudreau, L. Broglia, A. Brunengo, H. Burkhardt, S. Chauvie, J. Chuma, R. Chytracek, G. Cooperman, G. Cosmo *et al.*, Nucl. Instrum. Methods Phys. Res., Sect. A **506**, 250 (2003).
[39] B. Sulignano, S. Heinz, F. P. Heßberger, S. Hofmann, D. Ackermann, S. Antalic, B. Kindler, I. Kojouharov, P. Kuusiniemi, B. Lommel, R. Mann, K. Nishio, A. Popeko, S. Saro, B. Streicher, M. Venhart, and A. Yeremin, Eur. Phys. J. A **33**, 327 (2007).
[40] A. Lopez-Martens, T. Wiborg-Hagen, K. Hauschild, M. Chelnokov, V. Chepigin, D. Curien, O. Dorvaux, G. Drafta, B. Gall, A. Görgen, M. Guttormsen, A. Isaev, I. Izosimov, A. Kabachenko, D. Katrasev, T. Kutsarova, A. Kuznetsov, A. Larsen, O. Malyshev, A. Minkova, S. Mullins, H. Nyhus, D. Pantelica, J. Piot, A. Popeko, S. Saro, N. Scintee, S. Siem, N. Syed, E. Sokol, A. Svirikhin, and A. Yeremin, Nucl. Phys. A **852**, 15 (2011).
[41] W. Nazarewicz, J. Dudek, R. Bengtsson, T. Bengtsson, and I. Ragnarsson, Nucl. Phys. A **435**, 397 (1985).
[42] H. Pradhan, Y. Nogami, and J. Law, Nucl. Phys. A **201**, 357 (1973).
[43] P. Möller and J. Nix, Nucl. Phys. A **536**, 20 (1992).
[44] W. Myers and W. Swiatecki, Nucl. Phys. **81**, 1 (1966).
[45] P. T. Greenlees, R.-D. Herzberg, S. Ketelhut, P. A. Butler, P. Chowdhury, T. Grahn, C. Gray-Jones, G. D. Jones, P. Jones, R. Julin, S. Juutinen, T.-L. Khoo, M. Leino, S. Moon, M. Nyman, J. Pakarinen, P. Rahkila, D. Rostron, J. Sarén *et al.*, Phys. Rev. C **78**, 021303(R) (2008).
[46] R. R. Chasman, I. Ahmad, A. M. Friedman, and J. R. Erskine, Rev. Mod. Phys. **49**, 833 (1977).
[47] P. Möller, A. Sierk, T. Ichikawa, and H. Sagawa, At. Data Nucl. Data Tables **109-110**, 1 (2016).
[48] X.-T. He, S.-Y. Zhao, Z. Zhen-Hua, and Z.-Z. Ren, Chin. Phys. C **44**, 034106 (2020).
[49] J.-P. Delaroche, M. Girod, H. Goutte, and J. Libert, Nucl. Phys. A **771**, 103 (2006).
[50] S. K. Tandel, T. L. Khoo, D. Seweryniak, G. Mukherjee, I. Ahmad, B. Back, R. Blinstrup, M. P. Carpenter, J. Chapman, P. Chowdhury, C. N. Davids, A. A. Hecht, A. Heinz, P. Ikin, R. V. F. Janssens, F. G. Kondev, T. Lauritsen, C. J. Lister, E. F. Moore, D. Peterson, P. Reiter, U. S. Tandel, X. Wang, and S. Zhu, Phys. Rev. Lett. **97**, 082502 (2006).
[51] M. Asai, F. P. Heßberger, and A. Lopez-Martens, Nucl. Phys. A **944**, 308 (2015), Special Issue on Superheavy Elements.